ELSEVIER

Atmospheric Research 71 (2004) 171–192

ATMOSPHERIC RESEARCH

www.elsevier.com/locate/atmos

Estimating the atmospheric water vapor content from multi-filter rotating shadow-band radiometry at São Paulo, Brazil

Artemio Plana-Fattori[a,*], Philippe Dubuisson[b,1], Boris A. Fomin[c,2], Marcelo de Paula Corrêa[a,d,3]

[a] *Departamento de Ciências Atmosféricas, Instituto de Astronomia, Geofisica e Ciências Atmosféricas, Universidade de São Paulo (USP), São Paulo, Brazil*

[b] *UMR CNRS 8013 ELICO, Université du Littoral Côte d'Opale, Wimereux, France*

[c] *Russian Research Center "Kurchatov Institute" Moscow, Russian Federation*

[d] *Divisao de Satelites e Sistemas Ambientas Centro de Previsão de Tempo e Estudos Climáticos, Instituto Nacional de Pesquisas Espaciais, Cachoeira Paulista, Brazil*

Received 9 July 2003; received in revised form 19 January 2004; accepted 24 February 2004

Abstract

Selected measurements performed with Multi-Filter Rotating Shadow-band Radiometers under cloudless conditions at an urban tropical site, São Paulo, Brazil (23.65°S, 46.62°W, 800 m above the mean sea level) are analyzed. Water vapor content (U) values are estimated from the analysis of measurements performed near 940 nm with two bandwidths (10 and 35 nm). Narrow- and wide-band measurements performed near 940 nm are analyzed separately with the help of line-by-line radiative model computed transmittances, allowing independent $\hat{U}_N$ and $\hat{U}_W$ estimates. The ratio of these measurements is also analyzed, allowing a third water vapor content estimate ($\hat{U}_{NW}$). Selected approaches for computing water vapor absorption are compared, including two line parameter databases and two line-by-line models. After pooling, all results obtained from measurements performed during 16 cloudless mornings and representing the water vapor absorption through HITRAN-2000 line parameters and CKD-2.4 continuum model, estimates $\hat{U}_N$, $\hat{U}_W$, and $\hat{U}_{NW}$ were on average 1.8, 0.5, and 4.0 kg m^{-2} lower than respective values provided by balloon-borne

* Corresponding author. Departamento de Geofísica, Universidad de Chile, Casilla 2777, 6511227 Santiago, Chile. Fax: +56-2-696-8790.

E-mail addresses: artemio@dgf.uchile.cl (A. Plana-Fattori), dub@mren2.univ-littoral.fr (P. Dubuisson), fomin@imp.kiae.ru (B.A. Fomin), mpcorrea@cptec.inpe.br (M. de Paula Corrêa).

[1] Fax: +33-3-2199-6401.

[2] Fax: +7-095-1941994.

[3] Fax: +55-12-3101-2835.

doi:10.1016/j.atmosres.2004.02.002

soundings, respectively; and $\hat{U}_N$ estimates were 3% to 14% smaller than respective $\hat{U}_W$ values. Assuming that the independent values provided by soundings are accurate, the ad hoc reduction of continuum absorption coefficients to 50% of values provided by CKD-2.4 model improved the reliability of narrow-band water vapor content estimates in this study. Lastly, the influence of aerosol extinction on water vapor content was minimized from the analysis of measurements performed near 870 and 1035 nm. The corresponding turbidity exponent α assumed values between 0.7 and 1.1, which is somewhat weaker than those usually reported for urban conditions.

Keywords: Solar transmission measurements; Near-infrared; Atmospheric water vapor content; Aerosol optical depth; Atmospheric turbidity; São Paulo (Brazil)

1. Introduction

Present climate conditions depend on the occurrence of water vapor (Harries, 1997). Estimates of the column-integrated water vapor content (U) are important to characterize the atmospheric state in energy and water budget studies on regional scale, as well as to minimize uncertainties in space geodesy and remote sensing applications. A number of approaches have been conceived with the aim of monitoring U through ground-based and space-borne radiation measuring systems. A number of these approaches are based on absorption of solar radiation in the atmosphere (King et al., 1992; Schmid et al., 2001). Global coverage is only possible with space borne instruments, and ground-based network measurements are required to validate those retrievals.

The measurement of solar beam transmittance constitutes one of the oldest passive techniques still in use for remote monitoring of the atmospheric aerosol in units of optical depth (Deirmendjian, 1980). Its information content has justified the implementation of a number of solar radiometer networks (see review by Holben et al., 2001). As a version of such a technique, the measurement of atmospheric transmittance within and adjacent to the central part of a water vapor absorption band in the near-infrared has been proposed for estimating the water vapor content in the atmosphere (Foskett and Foster, 1943). Despite its conceptual simplicity, this approach may provide biased U estimates when compared to those resulting from microwave radiometry, balloon-borne soundings, and analysis of Global Positioning System delays (e.g. Ingold et al., 2000). This is because atmospheric transmittances derived from solar radiometer measurements depend on the spectral characteristics of water vapor absorption, solar irradiance, and instrument response throughout the passbands under consideration. An accurate estimation of U is possible from a comparison between measured and line-by-line (LBL) radiative model computed transmittances (e.g. Ingold et al., 2000); however, U estimates become dependent on assumptions about line parameters (Schmid et al., 2001). On the other hand, the application of a LBL model with a given set of line parameters can allow different U estimates from measurements with different instruments (Schmid et al., 2001, 2003).

Multi-Filter Rotating Shadow-band Radiometers (MFRSR) similar to that developed by Harrison et al. (1994) have provided reliable measurements of direct-normal, total-horizontal and diffuse-horizontal irradiances near the ground at selected wavelength

passbands of the solar spectrum. The analysis of MFRSR measurements has provided aerosol optical depths as well as column-integrated contents of water vapor, ozone, and nitrogen dioxide (Michalsky et al., 1995; Alexandrov et al., 2002a,b).

In this article we present the first U estimates resulting from MFRSR measurements performed at São Paulo, Brazil. With more than 16 million inhabitants and 5 million automobiles, the metropolitan area around São Paulo is the largest industrial pole of South America. The semi-continuous operation of two MFRSR instruments started in November 1999 near a meteorological station at about 3 km from a routine balloon-borne sounding site. Both instruments were ordered with two wavelength passbands centered near 940 nm, associated with a wide bandwidth (35 nm) as proposed by Volz (1974) and with a narrow bandwidth (10 nm, full-width-at-half-maximum) as employed in some solar radiometer networks (e.g. Michalsky et al., 1995; Holben et al., 1998). Narrow- and wide-band measurements performed near 940 nm are analyzed separately and also in terms of their ratio as proposed by Frouin et al. (1990). These measurements are interpreted in terms of respective U estimates with the help of transmittances computed through LBL models. Both instruments were also ordered with two adjacent passbands associated with negligible water vapor absorption (near 870 and 1035 nm). Measurements performed with these adjacent passbands are used to minimize the influence of aerosol extinction on U estimates, as suggested by Thome et al. (1992).

Section 2 presents instruments and measurements under consideration. As described herein, only measurements performed between November 1999 and August 2000 under cloudless conditions during balloon-borne soundings were selected. Section 3 describes the methods employed for estimating U, including the analysis of water vapor passband transmittances computed according to selected approaches. In addition to the application of two LBL models with the same set of line parameters, and to the application of one of the models to two sets of line parameters, a sensitivity test about the magnitude of water vapor continuum absorption coefficients is performed. Section 4 analyzes the consistency of U estimates and the influence of assumptions used in water vapor absorption computations, including simultaneous measurements with both instruments in a few cases. Conclusions and future work are summarized in Section 5.

2. Instruments and measurements

2.1. Instruments

Harrison et al. (1994) have described in full detail the measurement concept and the implementation of the Multi-Filter Rotating Shadow-band Radiometer (MFRSR). Briefly, total-horizontal irradiances at selected wavelength passbands in the solar spectrum are measured with an array of photodiodes with interference filters, which are mounted inside a thermally insulated and temperature-controlled integrating cavity. The optical inlet is a diffuser made of Spectralon, an optical plastic resistant to weathering and ultraviolet degradation. Diffuse-horizontal irradiances are measured with the help of a shadowing band coupled with a stepping motor, itself controlled by a self-contained microprocessor. The sequence of measurements starts with the shadow-band at nadir, allowing total-horizontal

irradiances; then the band is rotated and stopped in order to allow three measurements, the middle one blocking the sun apparent disk. The other two measurements, blocking the sky 9° to either side from the sun position, permit a first-order correction for the excess of sky blocked by the shadow-band when the sun-blocking measurement is performed. Direct-normal irradiances are evaluated by subtracting diffuse-horizontal from total-horizontal irradiances and dividing the result by the cosine of the solar zenith angle.

One instrument MFRSR was operated between November 1999 and January 2002 on top of a 10-m-high building near the main meteorological station of the University of São Paulo (23.65°S, 46.62°W, 800 m above mean sea level). The building and the meteorological station are located within a park whose area is several square kilometers. A second instrument MFRSR was operated on the same building during selected periods of few weeks. The diffusers, when exposed to sunlight, have been cleaned as indicated by the instrument manufacturer (Yankee Environmental Systems, Turners Falls, MA, USA). Measurement sequences, including the detector assembly temperature, have been programmed to occur four times per minute; averages over four sequences have been stored.

Both instruments MFRSR were ordered with a nonstandard choice of wavelength passbands (see Table 1). This choice was guided by two reasons. First, additional efforts about the representation of the water vapor absorption were recommended by a previous study on U estimates from measurements with two passbands near 940 nm (Plana-Fattori et al., 1998). Second, the availability of two passbands at adjacent regions associated with negligible water vapor absorption (870 and 1035 nm) can minimize the aerosol extinction influence on U estimates, as suggested by Thome et al. (1992).

Measurements performed with both instruments MFRSR have been interpreted by applying the calibration constants provided by their manufacturer. These constants were obtained in December 1998, with the help of 1000-W calibrated NIST-traceable FEL lamps in laboratory (see http://www.yesinc.com/support/optcal/optcal.html). Caution has been recommended about the use of standard lamps in calibrating solar radiometers, in the sense that such results must be combined with Langley-plot calibrations (Schmid et al., 1998; Kiedron et al., 1999). The reliability associated with Langley-plot calibrations has been reduced at our MFRSR site, mainly because of the transient behavior that character-

Table 1
Equivalent center wavelengths (λ_K) and equivalent bandwidths (EB_K) associated with both MFRSR instruments under consideration, in nanometers

Passband	MFRSR s/n 434		MFRSR s/n 435		Standard	
	λ_K	EB_K	λ_K	EB_K	λ_K	$FWHM_K$
2	415.0	9.8	415.5	9.7	415	10
3	671.5	9.8	672.4	9.9	500	10
4	869.8	11.1	869.7	11.1	615	10
5	938.5	10.8	940.5	10.9	673	10
6	938.6	36.1	938.7	36.4	870	10
7	1036.7	11.9	1036.8	11.6	940	10

Last column presents the standard choice of wavelength passbands suggested by the instrument manufacturer, for which EB_K (integral of radiometric transmission efficiencies) is replaced by its nominal value, $FWHM_K$ (full-width-at-half-maximum).

izes the atmospheric turbidity in urban areas. In this article we apply the calibration constants provided by the manufacturer to the analysis of the measurements performed with instrument MFRSR s/n 435 during its first year of operation (November 1999 to October 2000), as well as to those performed with instrument MFRSR s/n 434 during its few weeks of operation in that period.

2.2. Measurements

In order to select the situations to be analyzed, we defined three conditions to simultaneously be met: (a) availability of measurements with at least one of the two MFRSR instruments, (b) availability of humidity profiles from balloon-borne soundings up to the tropopause or above, and (c) occurrence of cloudless conditions for at least two hours around the sounding start. A routine balloon-borne Vaisala RS80-15N sounding system was in operation at a distance of about 3 km from the MFRSR site until October 2000. Profiles were provided with no information about the period of storage of the radiosondes after manufacturer calibration. Hence, errors associated with relative humidity profiles cannot properly be assessed as recommended (Turner et al., 2003). The identification of cloudless conditions was assessed on hourly basis from human-made routine whole sky observations performed near the MFRSR site. Cloudiness conditions between November 1999 and October 2000 at São Paulo were such that only a few of the simultaneous MFRSR and soundings measurements occurred under cloudless conditions. Namely, there were 13 soundings performed simultaneously with measurements from MFRSR s/n 435, five from MFRSR s/n 434, and only two from both instruments. Water vapor content values resulting from soundings ranged from 2.4 to 25.5 kg m^{-2} for the aforementioned situations.

Table 2 presents the situations under consideration. Most of them correspond to autumn/winter conditions, as a direct consequence of the cloudiness annual cycle at São Paulo. The sounding starting time (UTC_S) also corresponds to the beginning of the period of 30 min during which the aerosol optical depth and the water vapor content estimates resulting from one-minute irradiances are averaged. Atmospheric pressure (not shown) was provided by the meteorological station near the MFRSR site.

Unfortunately, both instruments MFRSR have operated simultaneously on only two cloudless mornings (May 15 and June 06, 2000), separated by 3 weeks apart. The ratio of respective measurements of total-horizontal irradiances was less than unity from all 1-min irradiances, on both dates and for all the six passbands. In other words, lower irradiances were provided by the instrument MFRSR s/n 435, which was exposed to sunlight for longer periods since November 1999 than its twin. For the passbands centered near 670 and 870 nm, the ratio of irradiances was particularly consistent between the two dates: 0.943–0.949 (May 15) and 0.945–0.951 (June 06) for 670 nm; 0.945–0.952 (May 15) and 0.944–0.951 (June 06) for 870 nm. The worst results were observed for the passbands centered near 415 nm, for which that ratio assumed values ranging from 0.814 to 0.824 on May 15 and from 0.825 to 0.843 on June 06. Such ratios below unity cannot be translated in instrumental aging as a consequence of exposure to sunlight and operation, since the two MFRSR were not compared before. However, visual inspection of both instruments indicated that the diffuser of MFRSR s/n 434 had an appearance slightly whiter than its MFRSR s/n 435 counterpart in the period April–June 2000. On the other hand, the comparisons conducted

Table 2
Summary of situations analyzed in this study

Date (year/month/day)	UTC_S	U_S (kg m^{-2})	ΔZ_O (deg)	MFRSR (s/n)	α	β
1999/11/25	11^h32^m	13.1	39.6–46.5	435	0.8	0.23
1999/12/17	11^h31^m	19.3	41.4–48.2	435	0.7	0.21
2000/01/10	11^h31^m	25.5	44.2–51.0	435	0.7	0.22
2000/04/12	11^h33^m	14.8	55.5–61.6	434	0.8	0.19
2000/04/25	11^h34^m	9.2	57.6–63.3	434	1.1	0.17
2000/04/28	11^h31^m	11.9	58.6–64.4	434	0.9	0.15
2000/05/15	12^h56^m	21.3	48.8–52.7	434	0.8	0.31
				435	0.8	0.35
2000/06/06	11^h35^m	15.5	63.8–69.0	434	1.0	0.16
				435	1.0	0.18
2000/06/15	11^h37^m	15.3	64.2–69.3	435	1.1	0.19
2000/06/16	11^h34^m	14.0	64.7–69.9	435	1.1	0.17
2000/07/07	11^h58^m	12.9	60.9–65.9	435	0.9	0.16
2000/07/17	11^h57^m	2.4	60.2–65.3	435	1.1	0.15
2000/08/21	11^h44^m	9.0	55.7–61.5	435	0.9	0.20
2000/08/22	11^h32^m	9.9	57.7–63.7	435	1.0	0.22
2000/08/24	11^h32^m	14.3	57.2–63.2	435	1.0	0.24
2000/08/25	11^h30^m	14.3	57.3–63.4	435	0.9	0.23

Columns present: date, Universal Time at *s*ounding start (UTC_S), water vapor content provided by soundings (U_S), range of solar zenith angles during the first 30 min after the sounding start (ΔZ_O), the MFRSR instrument(s) which was(were) operating on the date under consideration, and turbidity parameters resulting from measurements near 870 and 1035 nm (see text).

on May 15 and June 06, 2000 show that the instrument MFRSR s/n 435 provided total-horizontal irradiances that were 15.7% to 18.6% smaller than those obtained with the MFRSR s/n 434 in the case of passbands centered near 415 nm, with no apparent reason.

This article analyzes MFRSR measurements performed with passbands centered near 870, 940, and 1035 nm only, and assuming valid the calibration constants that were provided by the instrument manufacturer. Such a choice can be justified firstly by the limited reliability of Langley-plots at the MFRSR site as the main approach for assessing calibration factors; and secondly by the present interest on water vapor content estimates.

3. Methods

3.1. Atmospheric transmittances

With no clouds in the equivalent field of view of the instrument (about 8° full width around the apparent sun disk; Michalsky et al., 1995), then direct-normal irradiances measured with the *K*-th passband of an instrument MFRSR can be expressed as:

$$S_K = \frac{\int_{\Delta\lambda_K} (1/d^2) \cdot I_O(\lambda) \cdot R_K(\lambda) \cdot T(\lambda) \cdot d\lambda}{\int_{\Delta\lambda_K} R_K(\lambda) \cdot d\lambda} \quad (1)$$

where d is the effective Sun–Earth distance in astronomical units; $I_O(\lambda)$ is the spectral irradiance associated with the solar constant; $R_K(\lambda)$ is the radiometric transmission efficiency; and $T(\lambda)$ is the (direct) total atmospheric transmittance for radiation of wavelength λ. Both integrals above are performed over the wavelength range $\Delta\lambda_K$ throughout which $R_K(\lambda)>0$. The ratio of irradiance S_K to its value $S_{O,K}$ at the top of the atmosphere gives the passband transmittance $T(\lambda_K)$, i.e. the mean value of $T(\lambda)$ weighted by solar spectral irradiances and radiometric transmission efficiency, where λ_K is the equivalent center wavelength. Passband transmittances depend on geophysical variables which are included in monochromatic transmittances $T(\lambda)$ (sun disk apparent position, atmospheric pressure, vertical distribution of gaseous absorbers and suspended particles, etc.), as well as on solar spectral irradiances and on instrument response.

Total passband transmittances $T(\lambda_K)$ may be represented by the product of three terms, namely the aerosol extinction, the water vapor absorption (H_2O), and *other* (remaining) processes:

$$T(\lambda_K) = T_{AER}(\lambda_K) \cdot T_{H2O}(\lambda_K) \cdot T_{OTHER}(\lambda_K) \tag{2}$$

In the case of MFRSR passbands centered near 870, 940, and 1035 nm, the computation of $T_{OTHER}(\lambda_K)$ might include weak absorption by ozone and oxygen as well as molecular scattering. As a matter of fact, only the latter has a significant influence on MFRSR measurements near 870, 940, and 1035 nm. The passband transmittance associated with each of these processes for each passband under consideration was computed as the mean value of the respective monochromatic transmittances weighted by solar spectral irradiances and radiometric transmission efficiency. In the case of molecular scattering, the computations considered sea level optical depths for the tropical atmospheric conditions given in Table 4 of Bucholtz (1995), corrected to actual values of atmospheric pressure at the MFRSR site. In the case of ozone absorption, computations were performed by considering cross-sections proposed by Shettle and Anderson (1995) and the tropical model atmosphere (McClatchey et al., 1972). At $Z_O = 60°$ (a typical solar zenith angle among the situations of interest, see Table 2), passband transmittances $T_{O3}(\lambda_K)$ were higher than 0.999 for the passbands centered near 870, 940, and 1035 nm. In the case of absorption by oxygen collision pairs (O_2–O_2), data and formulation proposed by Greenblatt et al. (1990) and Mlawer et al. (1998) as included in the CKD-2.4 continuum model were applied. Passband transmittances $T_{O2-O2}(\lambda_K)$ were higher than 0.999 at $Z_O = 60°$, even for the passband near 1035 nm. In the following, absorption by ozone as well as that by O_2–O_2 were assumed negligible for the passbands centered near 870, 940, and 1035 nm.

Water vapor passband transmittances are defined as:

$$T_{H2O}(\lambda_K) = \frac{\int_{\Delta\lambda_K} I_O(\lambda) \cdot R_K(\lambda) \cdot T_{H2O}(\lambda) \cdot d\lambda}{\int_{\Delta\lambda_K} I_O(\lambda) \cdot R_K(\lambda) \cdot d\lambda} \tag{3}$$

This equation can be applied to two passbands centered near 940 nm associated with different bandwidths, allowing narrow-$T_{H2O}(940_N)$ and wide-band $T_{H2O}(940_W)$ water

vapor transmittances; in this study, they correspond respectively to bandwidths of about 10 and 35 nm. Experimental evaluations of $T_{H2O}(940_N)$ and $T_{H2O}(940_W)$ were obtained as described below. Theoretical evaluations of $T_{H2O}(940_N)$ and $T_{H2O}(940_W)$ are analyzed in Section 3.2, with the help of line-by-line absorption calculations. Some of such calculations were performed for the passbands centered near 870 and 1035 nm, in order to assess the contribution of water vapor absorption to respective MFRSR measurements. Resulting passband transmittances $T_{H2O}(870)$ and $T_{H2O}(1035)$ were higher than 0.999 at $Z_O = 60°$ under tropical atmospheric conditions ($U = 41.9$ kg m^{-2}). Therefore, water vapor absorption was assumed negligible for these two passbands.

Aerosol extinction is almost neutral across bandwidths of few nanometers, hence passband transmittances $T_{AER}(\lambda_K)$ may be expressed as:

$$T_{AER}(\lambda_K) = \exp(-m \cdot \tau_{AER}(\lambda_K)) \tag{4}$$

where $m = m(Z_O)$ is the optical mass at solar zenith angle Z_O. Aerosol optical depths at $\lambda_K = 870$ and $\lambda_K = 1035$ nm are estimated from experimental passband transmittances $T(\lambda_K)$ and the computation of m and $T_{OTHER}(\lambda_K)$.

The accurate estimation of the water vapor content from solar transmission measurements near 940 nm requires the assessment of aerosol extinction (e.g. Thome et al., 1992). Because of its smooth spectral dependence in the vicinity of that absorption band, the following approximation was assumed valid for $\tau_{AER}(\lambda_K)$:

$$\tau_{AER}(\lambda_K) = \beta \cdot \lambda_K^{-\alpha} \tag{5}$$

where the exponent α and the coefficient β can be recognized as the turbidity parameters proposed by Ångström (e.g. Paltridge and Platt, 1976, pp. 225–226). These parameters can be straightforwardly evaluated after applying Eq. (5) to the aerosol optical depths estimated from measurements near 870 and 1035 nm.

In summary, experimental evaluations of narrow-band $T_{H2O}(940_N)$ and wide-band $T_{H2O}(940_W)$ transmittances associated with water vapor absorption were obtained by applying Eq. (2), i.e. dividing the experimental passband transmittances $T(940_N)$ and $T(940_W)$ by the respective product of $T_{OTHER}(\lambda_K)$ and $T_{AER}(\lambda_K)$. The latter were obtained by applying Eqs. (4) and (5), after the estimation of turbidity parameters α and β from measurements performed with the passbands centered near 870 and 1035 nm. These steps were applied to 1-min irradiances, corresponding to averages over four measurement sequences. For the sake of analysis, the resulting turbidity parameters and water vapor content estimates (see Section 3.2) were averaged over the first 30 min after the starting of the balloon-borne soundings presented in Table 2.

3.2. Absorption by water vapor

Water vapor narrow- ($T_{H2O}(940_N)$) and wide-band ($T_{H2O}(940_W)$) transmittances defined by Eq. (3) were computed through line-by-line spectral integration, by taking into account (i) the absorption spectrum resulting from the application of a given representation for the

water vapor absorption near 940 nm in a given LBL radiative model, (ii) the radiometric transmission efficiencies $R_K(\lambda)$ as provided by the instrument manufacturer, and (iii) the solar spectral irradiances $I_O(\lambda)$ resulting from the databases of M.E. Van Hoosier, H. Neckel and D. Labs, C. Wehrli, and M.P. Thekaekara, as contained in the LOWTRAN-7 radiative model (Kneizys et al., 1988). Sensitivity tests indicated that both passband transmittances become slightly smaller (0.3% or less) with negligible influence on water vapor content as estimated in this study, after replacing such solar spectral irradiances by those proposed by Kurucz (1994).

In order to compute realistic passband transmittances at the MFRSR site, the tropical model atmosphere (McClatchey et al., 1972) was adapted to a surface pressure of 0.9 atm, allowing a water vapor content $U^* = 26.91$ kg m^{-2}. The following solar zenith angles and water vapor contents were considered: Z_O=[0° (10°) 40° (5°) 60° (3°) 75°]; and $U = (j/8) \times U^*$, where $j = 1,\ldots, 10$.

Table 3 summarizes the approaches followed in computing water vapor passband transmittances. Results labeled F and D were obtained through updated versions of the line-by-line radiative models developed by Fomin (1995) and Dubuisson et al. (1996). Both models have provided reliable results in the scope of international comparisons, and previous versions of the latter have been employed in the development of methods for estimating the water vapor content from space-borne measurements of upward radiation near 940 nm (Bouffiès et al., 1997). In both models, the Lorentz line shape was modified as proposed by Clough et al. (1989), and any contributions beyond $+/-25$ cm^{-1} from the line center were excluded. Finally, the analysis of MFRSR measurements performed near 940 nm has suggested a far wing contribution absorption in this region that is between that computed by pure Lorentzian wings (non-continuum) and the CKD continuum (Vogelmann et al., 1998); in the last approach, continuum absorption coefficients provided by the model CKD-2.4 (Mlawer et al., 1999) were reduced to 50% of their values.

Table 4 presents some results corresponding to the instrument MFRSR s/n 435, under selected conditions of water vapor content and solar zenith angle. For the sake of comparison, the water vapor content and solar zenith angle conditions associated with the MFRSR measurements under consideration in this study were such that the water

Table 3
Summary of approaches followed in this study in computing water vapor passband transmittances near 940 nm

Approach	LBL model	Water vapor absorption spectrum
F1	Fomin (1995)	• line parameters from HITRAN-96 database (Rothman et al., 1998) • line intensities corrected as suggested by Giver et al. (2000) • continuum absorption coefficients as provided by the CKD-2.4 model
F2	Fomin (1995)	• line parameters from HITRAN – 2000 (Rothman et al., 2003) • continuum absorption coefficients as provided by the CKD-2.4 model
D2	Dubuisson et al. (1996)	• line parameters from HITRAN-2000 • continuum absorption coefficients as provided by the CKD-2.4 model
D3	Dubuisson et al. (1996)	• line parameters from HITRAN-2000 • continuum absorption coefficients : 50% of values provided by the CKD – 2.4 model

Underlines indicate changes from the previous approach.

Table 4
Water vapor passband transmittances near 940 nm evaluated according to four approaches (see Table 3)

Approach	F1	F2	D2	D3
$T_{H2O}(940_N)$				
Z_O=0°, U=(1/8)U*;	0.7221	0.7243	0.7267	0.7324
mU=3.364 kg m^{-2}	(−0.6%)	(−0.3%)		(+0.8%)
Z_O=0°, U=U*;	0.3200	0.3187	0.3221	0.3426
mU=26.91 kg m^{-2}	(−0.6%)	(−1.1%)		(+6.4%)
Z_O=75°, U=U*;	0.0714	0.0685	0.0741	0.0934
mU=102.6 kg m^{-2}	(−3.6%)	(−7.5%)		(+26%)
$T_{H2O}(940_W)$				
Z_O=0°, U=(1/8)U*;	0.7873	0.7911	0.7917	0.7959
mU=3.364 kg m^{-2}	(−0.6%)	(−0.1%)		(+0.5%)
Z_O=0°, U=U*;	0.4495	0.4528	0.4486	0.4643
mU=26.91 kg m^{-2}	(+0.2%)	(+1.0%)		(+3.5%)
Z_O=75°, U=U*;	0.1984	0.1979	0.1985	0.2168
mU=102.6 kg m^{-2}	(−0.1%)	(−0.3%)		(+9.2%)
$T_{H2O}(940_N)/T_{H2O}(940_W)$				
Z_O=0°, U=(1/8)U*;	0.9172	0.9156	0.9178	0.9202
mU=3.364 kg m^{-2}	(−0.1%)	(−0.2%)		(+0.3%)
Z_O=0°, U=U*;	0.7119	0.7037	0.7180	0.7378
mU=26.91 kg m^{-2}	(−0.8%)	(−2.0%)		(+2.8%)
Z_O=75°, U=U*;	0.3597	0.3461	0.3731	0.4310
mU=102.6 kg m^{-2}	(−3.6%)	(−7.2%)		(+16.%)

Radiometric transmission efficiencies were taken as provided by the manufacturer for the instrument MFRSR s/n 435. Figures between parentheses indicate relative differences from the respective D2 results; m is the optical mass at solar zenith angle Z_O, U_{H2O} is the water vapor content (kg m^{-2}), and U*=26.91 kg m^{-2}.

vapor content integrated along the optical path (the product mU) assumed values between 4.9 and 43.0 kg m^{-2}. Results in Table 4 can be summarized as follows.

• The overall water vapor absorption (lines and continuum contribution) is stronger for narrow- than for wide-band transmittances. It explains the fact that wide-band transmittances decrease more slowly than narrow-band transmittances with mU, and that $T_{H2O}(940_N)/T_{H2O}(940_W)$ is always smaller than unity.

• The application of HITRAN-2000 line parameters allowed a weak increase of high passband transmittance values and a weak decrease of low passband transmittance values (compare F1 and F2 results). Hence, theoretical values of $T_{H2O}(940_N)$ and $T_{H2O}(940_W)$ became more sensitive to changes in water vapor content after the replacement of corrected HITRAN-96 line parameters by those available in HITRAN-2000.

• Results labeled F2 and D2 were obtained after applying the same representation for the water vapor absorption in two different LBL models. Taking into account the whole set of conditions of water vapor content and solar zenith angle (see above), F2 and D2 results agree globally better for $T_{H2O}(940_W)$ than for $T_{H2O}(940_N)$. This indicates that the influence of LBL model parameters may decrease with the bandwidth under consideration.

• Results labeled D2 and D3 were obtained after applying the same line parameters in the same LBL model, but considering respectively 100% and 50% of the continuum

absorption coefficients provided by the model CKD-2.4. Narrow- and wide-band transmittances did increase after the reduction of continuum absorption coefficients. Moreover, such an increase depends itself on mU.

• We might expect that the influence of a given parameter on the computation of narrow- and of wide-band water vapor transmittances would be smoothed, perhaps counterbalanced, after the rationing of these passband transmittances. As shown in Table 4, theoretical values of $T_{H2O}(940_N)/T_{H2O}(940_W)$ are influenced by changes in line parameters (compare F1 and F2 results), changes in LBL model parameters (F2 and D2), and continuum absorption coefficients (D2 and D3). As a matter of fact, such a counterbalancing effect took place in a few cases only (e.g. F1 and F2 results, in the case where $mU \sim 3.3$ kg m^{-2}).

Water vapor passband transmittances depend nonlinearly on the water vapor content integrated along the optical path (Fig. 1). A number of groups working on U estimates from solar transmission measurements have applied parameterizations such as

$$\Theta_{H2O} = \exp\left(-A \cdot (m \cdot U)^B\right) \tag{6}$$

in approximating not only narrow-band transmittances ($\Theta_{H2O} = T_{H2O}(940_N)$) (e.g. Reagan et al., 1987) and wide-band transmittances ($\Theta_{H2O} = T_{H2O}(940_W)$) (Halthore et al., 1997) but also their ratio ($\Theta_{H2O} = T_{H2O}(940_N)/T_{H2O}(940_W)$) (Frouin et al., 1990). According to that approximation, a plot of $\ln(-\ln(\Theta_{H2O}))$ versus $\ln(mU)$ should provide a straight line whose slope is B and whose intercept is $\ln(A)$. Fig. 2 displays such a plot for the water vapor passband transmittances shown in Fig. 1. It seems that narrow-band only, and perhaps wide-band transmittances too, follows that linear behavior.

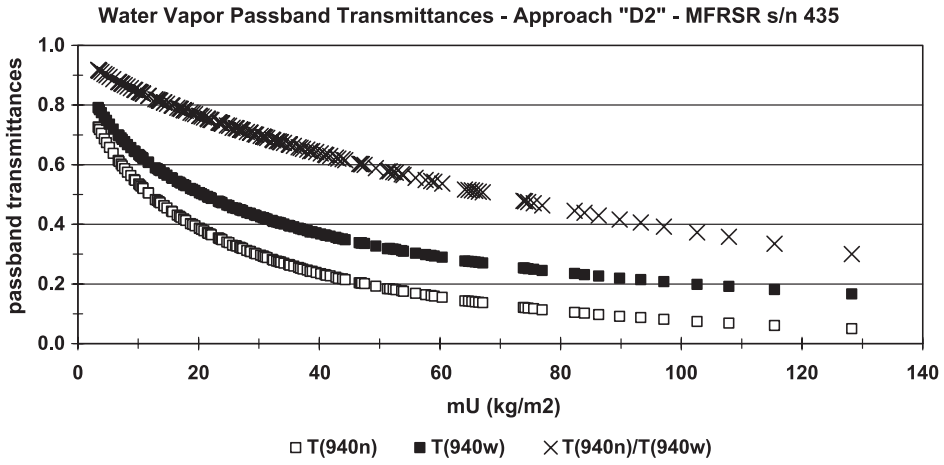

Fig. 1. Water vapor passband transmittances near 940 nm for instrument MFRSR s/n 435, evaluated according to a selected approach for computing water vapor absorption, as function of the water vapor content integrated along the optical path.

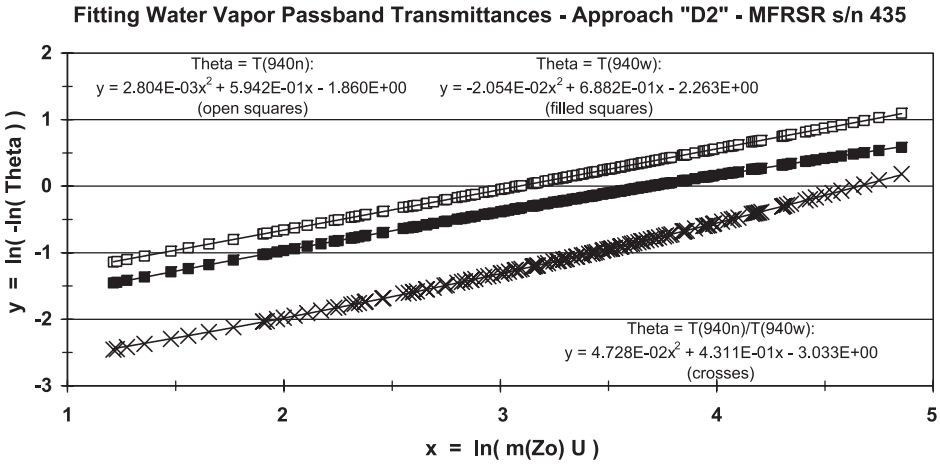

Fig. 2. Water vapor passband transmittances corresponding to Fig. 1, displayed in the scope of Eq. (7).

In order to apply a same strategy for the three passband transmittances, a higher-order relationship was assumed between $\ln(-\ln(\Theta_{\mathrm{H2O}})$ and $\ln(mU)$:

$$\ln(-\ln(\Theta_{\mathrm{H2O}})) = C_1 \cdot (\ln(m \cdot U))^2 + C_2 \cdot (\ln(m \cdot U)) + C_3 \tag{7}$$

Parameters C_1, C_2, and C_3 were evaluated through least squares fitting, taking into account each approach chosen for computing water vapor absorption as well as both passbands centered near 940 nm for each MFRSR instrument. Fig. 2 includes C_1, C_2, and C_3 values corresponding to $\Theta_{\mathrm{H2O}} = T_{\mathrm{H2O}}(940_{\mathrm{N}})$, $T_{\mathrm{H2O}}(940_{\mathrm{W}})$, and $T_{\mathrm{H2O}}(940_{\mathrm{N}})/T_{\mathrm{H2O}}(940_{\mathrm{W}})$ for approach D2, instrument MFRSR s/n 435. Similar values were obtained in the remaining cases (approaches, passbands, both instruments). The reliability of Eq. (7) can be presented in terms of the deviations observed between actual U values and their respective $\hat{U}$ estimates obtained through the inverse function of that approximation:

$$\hat{U} = (1/m) \cdot \exp\left(\frac{-C_2 + \sqrt{C_2^2 - 4 \cdot C_1 \cdot (C_3 - \ln(-\ln(\Theta_{\mathrm{H2O}})))}}{2 \cdot C_1}\right) \tag{8}$$

Taking into account all the U and Z_{O} values considered in computing the passband transmittances displayed in Figs. 1 and 2 (approach D2, instrument MFRSR s/n 435), the root mean square deviation reached 0.08, 0.10, and 0.11 kg m^{-2}, respectively, for $\Theta_{\mathrm{H2O}} = T_{\mathrm{H2O}}(940_{\mathrm{N}})$, $T_{\mathrm{H2O}}(940_{\mathrm{W}})$, and $T_{\mathrm{H2O}}(940_{\mathrm{N}})/T_{\mathrm{H2O}}(940_{\mathrm{W}})$. Moreover, the maximum absolute deviations were 0.34, 0.18, and 0.42 kg m^{-2}, respectively. Similar deviations were observed in the remaining cases.

4. Results

The consistency of water vapor content estimates $\hat{U}_N$, $\hat{U}_W$, and $\hat{U}_{NW}$ resulting from the analysis of transmittances $T_{H2O}(940_N)$, $T_{H2O}(940_W)$, and $T_{H2O}(940_N)/T_{H2O}(940_W)$, respectively, is hereafter discussed. The comparisons include the application of four approaches for computing water vapor absorption (F1, F2, D2, and D3, see Section 3.2), and values U_S provided by balloon-borne soundings. A number of reasons limit the accuracy of solar transmission measurements (e.g. Shaw, 1976). Besides such reasons, the option for discussing consistency rather than accuracy of U estimates can be justified by the limited accuracy of routine humidity profiles providing U_S values. The humidity profiles under consideration are probably less accurate than those obtained with research-grade measuring systems. For the sake of comparison, efforts conducted in the scope of the U.S. Department of Energy Atmospheric Radiation Measurement (ARM) program have shown that the mean bias between U estimates resulting from microwave radiometers and balloon-borne soundings may be as low as 2.5% although associated with one standard deviation of about 5% (see for example Fig. 10 of Revercomb et al., 2003).

Turbidity parameters α and β corresponding to every period of 30 min under consideration are summarized in Table 2. These results indicated $\tau_{AER}(500)$ values which were many times higher than aerosol background levels reported by other authors. For example, Holben et al. (2001) have reported $\tau_{AER}(500)$ values below 0.02 at the Mauna Loa Observatory (Hawaii, 3400 m a.m.s.l.) under pristine atmospheric conditions. The lowest value corresponding to Table 2 ($\tau_{AER}(500) \sim 0.3$) was associated with the exceptionally dry atmospheric conditions observed on July 17, 2000 (dew point temperatures of -2 °C near ground level at 12 UTC, and water vapor content of 2.4 kg m^{-2}).

Among the selected periods of 30 min here considered, those corresponding to May 15 and June 06, 2000 represent the only opportunities to compare aerosol optical depths resulting from both MFRSR instruments. As shown in Table 2, turbidity coefficients (β) from instrument MFRSR s/n 434 were lower than respective values from instrument MFRSR s/n 435. This is consistent because on both dates the latter provided irradiances lower than those of the former. On both dates the turbidity exponent (α) assumed almost the same value from both instruments. This can be interpreted by the fact that on both dates the aerosol optical depths near 870 and 1035 nm are not far apart.

It must be noted that, ideally, simultaneous estimates $\hat{U}_N$, $\hat{U}_W$, and $\hat{U}_{NW}$ would be equal to the respective U_S value: no experimental errors would be affecting neither MFRSR measurements nor balloon-borne soundings; and the approach for computing water vapor absorption would be consistent enough in order to allow not only the same U estimate from the analysis of $T_{H2O}(940_N)$, $T_{H2O}(940_W)$, and $T_{H2O}(940_N)/T_{H2O}(940_W)$ but also in agreement with the independent value provided by soundings.

Fig. 3 summarizes the results in 12 displays. The latter are presented in three rows (A, B, and C) and four columns (a, b, c, and d). The four columns present, respectively, the estimates $\hat{U}_N$, $\hat{U}_W$, and $\hat{U}_{NW}$, and the ratio $\hat{U}_N/\hat{U}_W$ as functions of the water vapor content value U_S provided by soundings. Each row corresponds to one representation for the water vapor absorption near 940 nm. Results in the first row (displays Aa–Ad) were obtained by taking into account HITRAN-96 line parameters after correction as suggested by Giver et al. (2000). HITRAN-2000 line parameters were used in the case of the second and third

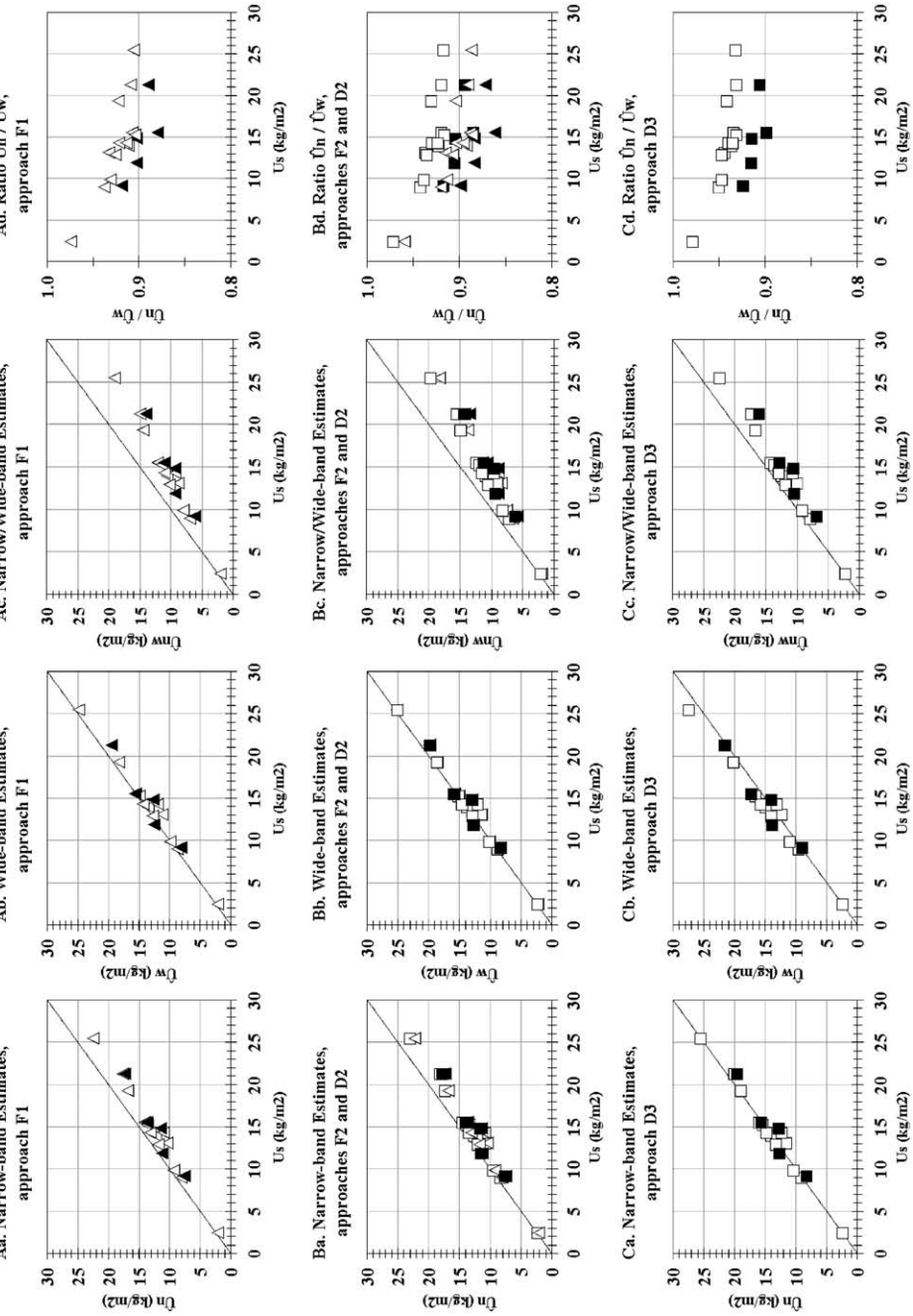
Aa. Narrow-band Estimates, approach F1
Ab. Wide-band Estimates, approach F1
Ac. Narrow/Wide-band Estimates, approach F1
Ad. Ratio Ûn / Ûw, approach F1
Ba. Narrow-band Estimates, approaches F2 and D2
Bb. Wide-band Estimates, approaches F2 and D2
Bc. Narrow/Wide-band Estimates, approaches F2 and D2
Bd. Ratio Ûn / Ûw, approaches F2 and D2
Ca. Narrow-band Estimates, approach D3
Cb. Wide-band Estimates, approach D3
Cc. Narrow/Wide-band Estimates, approach D3
Cd. Ratio Ûn / Ûw, approach D3
Ûn (kg/m2)
Ûw (kg/m2)
Ûnw (kg/m2)
Ûn / Ûw
Us (kg/m2)

rows (displays Ba–Cd). Results in the two first rows (displays Aa–Bd) were obtained by assuming continuum absorption coefficients as provided by the CKD-2.4 model, whereas these coefficients were divided by two in the third row (displays Ca–Cd). Triangles and squares correspond to the application of passband transmittances computed through the LBL models developed by Fomin (1995) and by Dubuisson et al. (1996), respectively. Filled and open symbols correspond to measurements performed with the instruments MFRSR s/n 434 and 435, respectively. Estimates $\hat{U}_N$, $\hat{U}_W$, and $\hat{U}_{NW}$ were obtained after applying Eq. (8) with respective values for parameters C_1, C_2, and C_3 corresponding to each case under consideration (approach for computing water vapor absorption, passband, and instrument).

The replacement of corrected HITRAN-96 line parameters by those available in HITRAN-2000 allowed almost the same $\hat{U}_N$ and $\hat{U}_W$ values, being that the ratio $\hat{U}_N/\hat{U}_W$ decreased slightly (compare triangles in displays Ad and Bd). The impact on $\hat{U}_N$ was smaller than that associated with the replacement of the LBL model of Fomin (1995) by that of Dubuisson et al. (1996) in computing water vapor absorption (compare triangles and squares in display Ba). Such a replacement of LBL model is more evident in terms of the ratio $\hat{U}_N/\hat{U}_W$ (compare triangles and squares in display Bd).

The reduction of absorption coefficients provided by the CKD-2.4 continuum model to 50% of their values allowed an increase in $\hat{U}_N$ and $\hat{U}_W$ (compare squares in displays Ba and Ca, and in Bb and Cb), because the same experimental transmittances were compared with theoretical values obtained by assuming less absorption per unit of water vapor content. Assuming that the U_S values provided by soundings were accurate, the reduction of continuum absorption coefficients did improve $\hat{U}_N$ estimates. In the case of measurements with the instrument MFRSR s/n 435, deviations between $\hat{U}_N$ and U_S became smaller (on average, from -10% to -2%) while the deviations between $\hat{U}_W$ and U_S changed their typical signal (on average, from -4% to $+4\%$). Moreover, $\hat{U}_N$ and $\hat{U}_W$ estimates became closer: on average, $\hat{U}_N/\hat{U}_W$ increased from 0.93 to 0.94.

Estimates $\hat{U}_{NW}$ resulting from the comparison between experimental and theoretical values of $T_{H2O}(940_N)/T_{H2O}(940_W)$ exhibited, in almost all the cases, larger deviations than $\hat{U}_N$ and $\hat{U}_W$ estimates when compared with U_S values (compare the first three columns in Fig. 3). The analysis of this result is not straightforward. First, experimental values of $T_{H2O}(940_N)$ and $T_{H2O}(940_W)$ for a given MFRSR were obtained from measurements with independent detectors, one for each passband. Hence, random experimental errors affecting $T_{H2O}(940_N)$ and $T_{H2O}(940_W)$ could enlarge uncertainties associated with $\hat{U}_{NW}$ estimates. The fact that $\hat{U}_N$ estimates were always smaller than respective $\hat{U}_W$ values (see the fourth column in Fig. 3) suggests that one relevant, systematic uncertainty remains to be assessed. Instrument calibration cannot be discarded as a reason. Second, uncertainties affecting a given approach for computing water vapor absorption could be partially cancelled after rationing theoretical values of $T_{H2O}(940_N)$ and $T_{H2O}(940_W)$. In reality,

Fig. 3. Water vapor contents estimated from narrow- and wide-band measurements near 940 nm after assuming selected approaches for computing water vapor absorption, as function of independent values resulting from sounding. Triangles and squares indicate results achieved from transmittances computed through the LBL models developed by Fomin (1995) and by Dubuisson et al. (1996). Filled and open symbols indicate results achieved from measurements performed with the instruments MFRSR s/n 434 and 435, respectively.

these theoretical values depend on a number of factors, and such a canceling rarely takes place (Table 4). However, the best $\hat{U}_{NW}$ estimates resulted from approach D3, whose continuum absorption coefficients were weaker than those considered by the other approaches (see display Cc in Fig. 3).

Lastly, among the periods of 30 min considered in this study (Table 2), those corresponding to May 15 and June 06, 2000 represented the only opportunities to compare $\hat{U}_N$, $\hat{U}_W$ and $\hat{U}_{NW}$ values resulting simultaneously from both MFRSR instruments with an independent value provided by sounding under cloudless conditions. Table 5 summarizes the results achieved by assuming the same representation for the water vapor absorption (HITRAN-2000 line parameters, CKD-2.4 continuum model) in both LBL models. Wide-band estimates $\hat{U}_W$ were robust: they did agree better than the respective $\hat{U}_N$ and $\hat{U}_{NW}$, either from different approaches or from different instruments.

The influence of temperature on passband and transmission of interference filters was one reason presented by Harrison et al. (1994) in justifying temperature stabilization of the MFRSR detector assembly. Further, passband and transmission of interference filters may shift in wavelength and change its shape over time. This effect has been documented for other solar radiometers (e.g. Table 1 of Schmid et al., 1998; Fig. 3 of Plana-Fattori et al., 1998). The aging of interference filters may introduce errors in U estimates from transmission measurements near 940 nm, even after the rationing of passband transmittances (Plana-Fattori et al., 1998). The influence of passband shifts in wavelength on U estimates seems to depend on a number of factors (Ingold et al., 2000).

An attempt in assessing the influence of passband shifts in wavelength on $\hat{U}_N$, $\hat{U}_W$, and $\hat{U}_{NW}$ estimates is presented below. Only the approach D2 for computing passband

Table 5
Comparison of U estimates resulting from both MFRSR instruments under selected conditions, taking into account two approaches for computing water vapor absorption (F2 and D2, see Table 3)

	May 15, 2000; from 12^h56^m to 13^h26^m UTC					
	U_S=21.3 kg m^{-2}					
	Instrument MFRSR s/n 434			Instrument MFRSR s/n 435		
Approach	$\hat{U}_N$	$\hat{U}_W$	$\hat{U}_{NW}$	$\hat{U}_N$	$\hat{U}_W$	$\hat{U}_{NW}$
F2	17.3	19.8	13.5	17.6	19.8	14.3
	(−4.0)	(−1.5)	(−7.8)	(−3.7)	(−1.5)	(7.0)
D2	17.7	19.8	14.3	18.1	19.7	15.4
	(−3.6)	(−1.5)	(−7.0)	(−3.2)	(−1.6)	(−5.9)
	June 06, 2000; from 11^h35^m to 12^h05^m UTC					
	U_S=15.5 kg m^{-2}					
	Instrument MFRSR s/n 434			Instrument MFRSR s/n 435		
Approach	$\hat{U}_N$	$\hat{U}_W$	$\hat{U}_{NW}$	$\hat{U}_N$	$\hat{U}_W$	$\hat{U}_{NW}$
F2	13.7	15.8	10.6	14.0	15.7	11.5
	(−1.8)	(+0.3)	(−4.9)	(−1.5)	(+0.2)	(−4.0)
D2	14.0	15.8	11.3	14.4	15.6	12.5
	(−1.5)	(+0.3)	(−4.2)	(−1.1)	(+0.1)	(−3.0)

Figures between parentheses indicate differences from the respective U_S values provide by soundings.

transmittances was taken into account; and radiometric transmission efficiencies provided by the manufacturer for both passbands of the instrument MFRSR s/n 435 were submitted to shifts in wavelength with no change in their shape. Fig. 4 summarizes the results achieved, as in Fig. 3. Here, the three rows correspond to the application of radiometric efficiencies as provided by the instrument manufacturer (+0), and to the application of those efficiencies after shifts of +2 and +4 nm (rows +2 and +4). For clarity, the vertical axis was extended in some displays. Symbols in the first row of Fig. 4 correspond to open squares in the second row of Fig. 3.

Theoretical narrow-band transmittances experienced an increase after both shifts in wavelength (results not shown). Narrow-band estimates $\hat{U}_N$ increased (see displays in the first column of Fig. 4) because they result from the same experimental narrow-band transmittances. Similarly, wide-band estimates $\hat{U}_W$ decreased (see displays in the second column) because theoretical wide-band transmittances decreased after both shifts in wavelength. The relatively high spectral dependence of line absorption seems to be the main reason for these results. Assuming the same shift in wavelength for both radiometric efficiencies provided by the manufacturer, the theoretical values of the ratio $T_{H2O}(940_N)/T_{H2O}(940_W)$ increased as a consequence of the increase of $T_{H2O}(940_N)$ and the decrease of $T_{H2O}(940_W)$. Narrow-to-wide-band estimates $\hat{U}_{NW}$ increased, "crossing" the one-to-one line with independent values provided by soundings (compare displays +0c and +2c). A similar remark could be applied to the values assumed by the ratio $\hat{U}_N/\hat{U}_W$, below and then above unity (compare displays +0d and +2d).

Although these results correspond to a particular approach for computing water vapor absorption near 940 nm, we cannot discard the occurrence of actual small shifts in wavelength affecting the passbands under consideration. Fig. 4 suggests that almost identical U estimates from $T_{H2O}(940_N)$, $T_{H2O}(940_W)$ and $T_{H2O}(940_N)/T_{H2O}(940_W)$ might be achieved after assuming a pair of relatively small (1 nm or less) shifts in wavelength, one affecting the narrow band, another affecting the wide band.

5. Summary and future work

The present article presented the first results regarding water vapor content estimates from measurements performed in the near-infrared with MFRSR instruments at São Paulo, Brazil. The interpretation of measurements performed with a narrow (10 nm) and a wide (35 nm) passband centered near 940 nm provided different narrow-band ($\hat{U}_N$), wide-band ($\hat{U}_W$), and narrow-to-wide-band estimates ($\hat{U}_{NW}$), which in turn were different from respective values provided by soundings (U_S).

The monitoring of the water vapor content from solar transmission measurements depends on the reliability of calibration constants among other instrument characteristics (like passbands response). Despite the differences observed between respective irradiances measured on May 15 and June 06, 2000 with both MFRSR instruments (see Section 2), almost the same turbidity exponent α (see Table 2) and essentially the same U estimates (see Table 5) were obtained. Instrument characteristics may change in time, affecting the accuracy of measurements and hence that of resulting water vapor content estimates (e.g., Plana-Fattori et al., 1998). When such an influence is not observed, the reason may be a

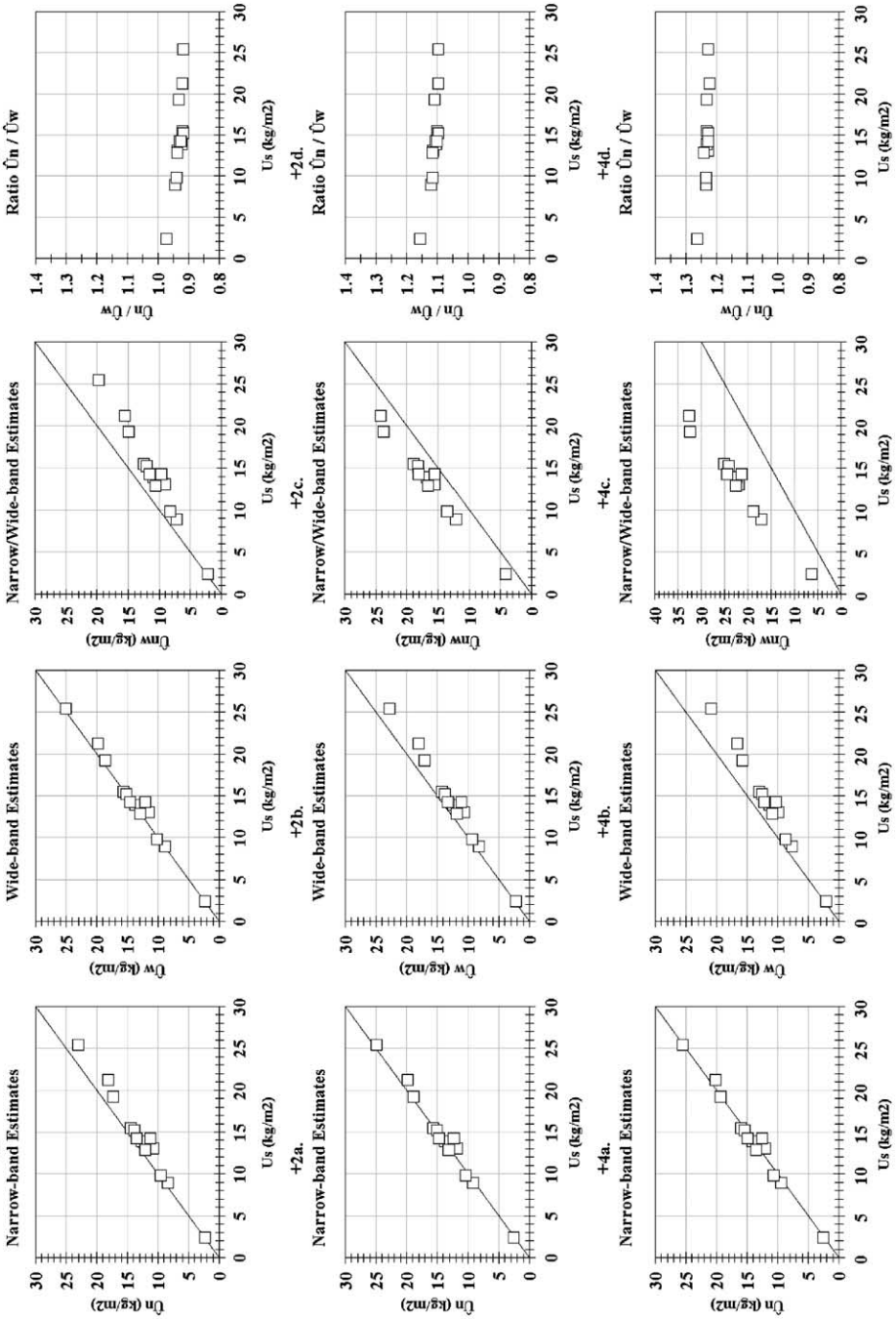
+0a.
Narrow-band Estimates
+0b.
Wide-band Estimates
+0c.
Narrow/Wide-band Estimates
+0d.
Ratio Ûn / Ûw
+2a.
Narrow-band Estimates
+2b.
Wide-band Estimates
+2c.
Narrow/Wide-band Estimates
+2d.
Ratio Ûn / Ûw
+4a.
Narrow-band Estimates
+4b.
Wide-band Estimates
+4c.
Narrow/Wide-band Estimates
+4d.
Ratio Ûn / Ûw
Ûn (kg/m2)
Ûw (kg/m2)
Ûnw (kg/m2)
Ûn / Ûw
Us (kg/m2)

fortuitous combination of independent effects. Future work regarding the analysis of MFRSR measurements in São Paulo depends on the assessment of instrument stability. Comparisons as those reported in this study may be useful, as a complement to instrument recalibration by the manufacturer.

In summary, estimates $\hat{U}_N$, $\hat{U}_W$, and $\hat{U}_{NW}$ were on average 1.8, 0.5, and 4.0 kg m^{-2} (i.e. 12%, 4%, and 27%) lower than values provided by soundings, after combining the results obtained from measurements performed with both MFRSR instruments and applying both LBL models with the second representation for the water vapor absorption (HITRAN-2000 line parameters, continuum absorption coefficients as provided by the CKD-2.4 model). Taking into account this representation for the water vapor absorption, the mean difference between the respective estimates $\hat{U}_N$, $\hat{U}_W$, and $\hat{U}_{NW}$ from the application of the two LBL models was -0.3, $+0.04$, and -0.7 kg m^{-2} (i.e. -3%, $+0.2\%$, and -7%). Taking into account a given LBL model, the replacement of corrected HITRAN-96 line parameters by those available in the database HITRAN-2000 allowed, on average, the decrease of estimates $\hat{U}_N$ and $\hat{U}_{NW}$ (by 0.1 and 0.4 kg m^{-2}, i.e. 0.5% and 4%) and the increase of estimates $\hat{U}_W$ (by 0.2 kg m^{-2}, i.e. 2%). The reduction of water vapor continuum absorption coefficients provided by the model CKD-2.4 to 50% of their values allowed the increase of estimates $\hat{U}_N$, $\hat{U}_W$, and $\hat{U}_{NW}$ on average by 1.3, 1.2, and 1.3 kg m^{-2}, i.e. 10%, 9%, and 12%. Such a reduction is consistent with efforts in constraining the magnitude of a water vapor continuum near 940 nm (Vogelmann et al., 1998). As a consequence, estimates $\hat{U}_N$ and $\hat{U}_W$ became slightly closer. Assuming that the values U_S provided by soundings are accurate, such a reduction of water vapor continuum absorption coefficients improved the reliability of estimates $\hat{U}_N$. Looking ahead and in order to clarify our findings, the strategy involving simultaneous estimates $\hat{U}_N$ and $\hat{U}_W$ must be tested using an independent measuring system that effectively provides accurate water vapor contents.

MFRSR measurements corresponding to different passbands are performed with independent detectors, hence experimental evaluations of $T_{H2O}(940_N)$ and $T_{H2O}(940_W)$ can be interpreted as two simultaneous, independent measures of water vapor absorption. The ratio of these passband transmittances might represent a third (dependent) measure of water vapor absorption. Narrow-to-wide-band estimates $\hat{U}_{NW}$ above exhibited, in almost all the cases, larger deviations than $\hat{U}_N$ and $\hat{U}_W$ estimates when compared with U_S values. On the other hand, it has been shown that slightly biased U estimates (about 0.1 kg m^{-2}) can be obtained from the ratio of passband transmittances resulting from measurements performed with instruments employing a filter wheel in front of a detector (Plana-Fattori et al., 1998). Therefore, the reliability of the narrow-to-wide-band approach seems more dependent on instrument concept than initially expected.

Wide-band water vapor content estimates were more robust than estimates $\hat{U}_N$ and $\hat{U}_{NW}$, in the sense that they presented smaller dependence with LBL model, with line parameters, and with actual instrument responses. The implementation of a similar wide-

Fig. 4. Water vapor contents estimated from narrow- and wide-band measurements near 940 nm after assuming the approach D2 for computing water vapor absorption and taking into account measurements performed with the instrument MFRSR s/n 435 only, as function of independent values resulting from sounding. The "rows" +0, +2, and +4 correspond, respectively, to shifts in wavelength of zero, +2, and +4 nm on radiometric efficiencies of both passbands.

passband near 940 nm in other instrument concepts is here suggested, because its potential application in solar radiometer networks.

Under a number of points of view, this study may be considered complementary to that achieved by Alexandrov et al. (2002a,b). Those authors successfully applied the fact that MFRSR instruments enables the measurement of direct-normal and diffuse-horizontal irradiances with the same detector in developing an algorithm that provides retrieval of aerosol properties and NO_2 and O_3 contents together with the determination of the instrument calibration constants. In this study, nonstandard passbands were employed and methods conceived with the aim of estimating the water vapor content were proposed. Much effort remains to be accomplished in testing the strategy involving two different bandwidths in a water vapor absorption band in the near infrared. Further, it might represent an additional opportunity to assess the consistency of representations for the water vapor absorption spectrum, as a complement of measurements performed nowadays in different near-infrared bands (e.g. Ingold et al., 2000).

Acknowledgements

The first named author thanks the Université du Littoral Côte d'Opale who kindly received him as a visiting scientist in January 2003. The authors thank S.A. Clough (Atmospheric and Environmental Research) for help with the CKD-2.4 continuum model; Eric P. Shettle (Naval Research Laboratory, Washington, DC) for help with ozone absorption cross-sections; Lee Harrison and Joe Michalsky (State University of New York at Albany), Maria Assunção Faus da Silva Dias and Pedro Leite da Silva Dias (USP) for helpful discussions; Simone Marilene Sievert da Costa, Nilson Luiz Neres, and Carlos Teixeira de Oliveira (USP) for help with instrument operation; Marcelo Cavedon Presti, Paulo Takeshi Matsuo, and Gilson Feitosa for help with balloon-borne sounding data; the staff of the meteorological station (USP) nearby the MFRSR site; the MFRSR manufacturer for its assistance; and the Brazilian agency FAPESP for financial support. Final acknowledgments are addressed to two anonymous reviewers, whose constructive criticism was decisive for the improvement of our manuscript; to Rosana Nieto Ferreira for her friendly help in the review of the English; and to Departamento de Geofísica of the Universidad de Chile, where the manuscript was revised.

References

Alexandrov, M.D., Lacis, A.A., Carlson, B.E., Cairns, B., 2002a. Remote sensing of atmospheric aerosols and trace gases by means of multifilter rotating shadowband radiometer. Part I: retrieval algorithm. J. Atmos. Sci. 59, 524–543.

Alexandrov, M.D., Lacis, A.A., Carlson, B.E., Cairns, B., 2002b. Remote sensing of atmospheric aerosols and trace gases by means of multifilter rotating shadowband radiometer. Part II: climatological applications. J. Atmos. Sci. 59, 544–566.

Bouffiès, S., Bréon, F.M., Tanré, D., Dubuisson, P., 1997. Atmospheric water vapor estimate by a differential absorption technique with the polarisation and directionality of the Earth reflectances (POLDER) instrument. J. Geophys. Res. 102, 3831–3841.

Bucholtz, A., 1995. Rayleigh-scattering calculations for the terrestrial atmosphere. Appl. Opt. 34, 2765–2773.

Clough, S.A., Kneizys, F.X., Davies, R.W., 1989. Line shape and the water vapor continuum. Atmos. Res. 23, 229–241.

Deirmendjian, D., 1980. A survey of light-scattering techniques used in the remote monitoring of atmospheric aerosols. Rev. Geophys. Space Phys. 18, 341–360.

Dubuisson, P., Buriez, J.C., Fouquart, Y., 1996. High spectral resolution solar radiative transfer in absorbing and scattering media: application to the satellite simulation. J. Quant. Spectrosc. Radiat. Transfer 55, 103–126.

Fomin, B.A., 1995. Effective interpolation technique for line-by-line calculations of radiation absorption in gases. J. Quant. Spectrosc. Radiat. Transfer 53, 663–669.

Foskett, L.W., Foster, N.B., 1943. A spectroscopic hygrometer. Bull. Am. Meteorol. Soc. 24, 146–153.

Frouin, R., Deschamps, P.-Y., Lecomte, P., 1990. Determination from space of atmospheric total water vapor amounts by differential absorption near 940 nm: theory and airborne verification. J. Appl. Meteorol. 29, 448–460.

Giver, L.P., Chakerian Jr., C., Varanasi, P., 2000. Visible and near-infrared $H_2^{16}O$ line intensity corrections for HITRAN-96. J. Quant. Spectrosc. Radiat. Transfer 66, 101–105.

Greenblatt, G.D., Orlando, J.J., Burkholder, J.B., Ravishankara, A.R., 1990. Absorption measurements of oxygen between 330 and 1140 nm. J. Geophys. Res. 95, 18577–18582.

Halthore, R.N., Eck, T.F., Holben, B.N., Markham, B.L., 1997. Sun photometric measurements of atmospheric water vapor column abundance in the 940-nm band. J. Geophys. Res. 102, 4343–4352.

Harries, J.E., 1997. Atmospheric radiation and atmospheric humidity. Q. J. Royal Meteorol. Soc. 123, 2173–2186.

Harrison, L., Michalsky, J., Berndt, J., 1994. Automated multifilter rotating shadow-band radiometer: an instrument for optical depth and radiation measurements. Appl. Opt. 33, 5118–5125.

Holben, B.N., Eck, T.F., Slutsker, I., Tanré, D., Buis, J.P., Setzer, A., Vermote, E., Reagan, J.A., Kaufman, Y.J., Nakajima, T., Lavenu, F., Jankowiak, I., Smirnov, A., 1998. AERONET: a federated instrument network and data archive for aerosol characterization. Remote Sens. Environ. 66, 1–16.

Holben, B.N., Tanré, D., Smirnov, A., Eck, T.F., Slutsker, I., Abuhassan, N., Newcomb, W.W., Schafer, J., Chatenet, B., Lavenu, F., Kaufman, Y.J., Vande Castle, J., Setzer, A., Markham, B., Clark, D., Frouin, R., Halthore, R.N., Karnieli, A., O'Neill, N.T., Pietras, C., Pinker, R.T., Voss, K., Zibordi, G., 2001. An emerging ground-based aerosol climatology. J. Geophys. Res. 106, 12067–12097.

Ingold, T., Schmid, B., Mätzler, C., Demoulin, P., Kämpfer, N., 2000. Modeled and empirical approaches for retrieving atmospheric water vapor content from solar transmittance measurements in the 0.72, 0.82, and 0.94 μm absorption bands. J. Geophys. Res. 105, 24327–24343.

Kiedron, P.W., Michalsky, J.J., Berndt, J.L., Harrison, L.C., 1999. Comparison of spectral irradiance standards used to calibrate shortwave radiometers and spectro-radiometers. Appl. Opt. 38, 2432–2439.

King, M.D., Kaufman, Y.J., Menzel, W.P., Tanré, D., 1992. Remote sensing of cloud, aerosol, and water vapor properties from the moderate resolution imaging spectrometer (MODIS). IEEE Trans. Geosci. Remote Sens. 30, 2–27.

Kneizys, F.X., Shettle, E.P., Abreu, L.W., Chetwynd, J.H., Anderson, G.P., Gallery, W.O., Selby, J.E.A., Clough, S.A., 1998. Users Guide to LOWTRAN-7. Air Force Geophysics Laboratory, Hanscom Air Force Base, publication AFGL-TR-88-0177 Environmental Research Papers No. 1010. 137 pp.

Kurucz, R.L., 1994. Synthetic infrared spectra. In: Rabin, D.M., Jefferies, J.T., Lindsey, C. (Eds.), Infrared Solar Physics (Proceedings of the 154th Symposium of the International Astronomical Union; Tucson, Arizona, March 2–6, 1992. Kluwer Academic Publishing, Dordrecht, pp. 523–531.

McClatchey, R.A., Fenn, R.W., Selby, J.E.A., Volz, F.E., Garing, J.S., 1972. Optical Properties of the Atmosphere, 3rd ed. Air Force Cambridge Research Laboratory, Hanscom Air Force Base publication AFCRL-72-0497, Air Force Cambridge Research Laboratory, Bedford, MA, 113 pp.

Michalsky, J.J., Liljegren, J.C., Harrison, L.C., 1995. A comparison of Sun photometer derivations of total column water vapor and ozone to standard measures of same at the Southern Great Plains atmospheric radiation measurement site. J. Geophys. Res. 100, 25995–26003.

Mlawer, E.J., Clough, S.A., Brown, P.D., Stephen, T.M., Landry, J.C., Goldman, A., Mucray, F.J., 1998. Observed atmospheric collision-induced absorption in near-infrared oxygen bands. J. Geophys. Res. 103, 3859–3863.

Mlawer, E.J., Clough, S.A., Brown, P.D., Tobin, D.C., 1999. Recent developments in the water vapor continuum. In: Burleigh, N., Carrothers, D. (Eds.), Annual ARM Science Team Meeting. U.S. Department of Energy, Richland, WA. pp. 1–66.

Paltridge, G.W., Platt, C.M.R., 1976. Radiative Processes in Meteorology and Climatology. Elsevier, Amsterdam. 318 pp.

Plana-Fattori, A., Legrand, M., Tanré, D., Devaux, C., Vermeulen, A., Dubuisson, P., 1998. Estimating the atmospheric water vapor content from Sun photometer measurements. J. Appl. Meteorol. 37, 790–804.

Reagan, J.A., Pilewskie, P.A., Scott-Fleming, I.C., Herman, B.M., Ben-David, A., 1987. Extrapolation of Earth-based solar irradiance measurements to exoatmospheric levels for broadband and selected absorption-band observations. IEEE Trans. Geosci. Remote Sens. GE-25, 647–653.

Revercomb, H.E., Turner, D.D., Tobin, D.C., Knuteson, R.O., Feltz, W.F., Barnard, J., Bosenberg, J., Clough, S., Cook, D., Ferrare, R., Goldsmith, J., Gutman, S., Halthore, R., Lesht, B., Liljegren, J., Linné, H., Michalsky, J., Morris, V., Porch, W., Richardson, S., Schmid, B., Splitt, M., Van Hove, T., Westwater, E., Whiteman, D., 2003. The ARM program's water vapor intensive observation periods: overview, initial accomplishments, and future challenges. Bull. Am. Meteorol. Soc. 84, 217–236.

Rothman, L.S., Rinsland, C.P., Goldman, A., Massie, S.T., Edwards, D.P., Flaud, J.M., Perrin, A., Camy-Peiret, C., Dana, V., Mandin, J.-Y., Schroeder, J., McCann, A., Gamache, R.R., Wattson, R.B., Yoshino, K., Chance, K.V., Jucks, K.W., Brown, L.R., Nemtchinov, V., Varanasi, P., 1998. The HITRAN molecular spectroscopic database and HAWKS (HITRAN Atmospheric Workstation): 1996 edition. J. Quant. Spectrosc. Radiat. Transfer 60, 665–710.

Rothman, L.S., Barbe, A., Benner, D.C., Brown, L.R., Camy-Peyret, C., Carleer, M.R., Chance, K., Clerbaux, C., Dana, V., Devi, V.M., Fayt, A., Flaud, J.-M., Gamache, R.R., Goldman, A., Jacquemart, D., Jucks, K.W., Lafferty, W.J., Mandin, J.-Y., Massie, S.T., Nemtchinov, V., Newnham, D.A., Perrin, A., Rinsland, C.P., Schroeder, J., Smith, K.M., Smith, M.A.H., Tang, K., Toth, R.A., Vander Auwera, J., Varanasi, P., Yoshino, K., 2003. The HITRAN molecular spectroscopic database: edition of 2000 including updates through 2001. J. Quant. Spectrosc. Radiat. Transfer 82, 5–44.

Schmid, B., Spyak, R.R., Biggar, S.F., Wehrli, C., Sekler, J., Ingold, T., Mätzler, C., Kämpfer, N., 1998. Evaluation of the applicability of solar and lamp radiometric calibrations of a precision Sun photometer operating between 300 and 1025 nm. Appl. Opt. 37, 3923–3941.

Schmid, B., Michalsky, J.J., Slater, D.W., Barnard, J.C., Halthore, R.N., Liljegren, J.C., Holben, B.N., Eck, T.F., Livingston, J.M., Russell, P.B., Ingold, T., Slutsker, I., 2001. Comparison of atmospheric water vapor content measurements from solar transmittance methods. Appl. Opt. 40, 1886–1896.

Schmid, B., Hegg, D.A., Wang, J., Bates, D., Redemann, J., Russell, P.B., Livingston, J.M., Jonsson, H.H., Welton, E.J., Seinfeld, J.H., Flagan, R.C., Covert, D.S., Dubovik, O., Jefferson, A., 2003. Column closure studies of lower tropospheric aerosol and water vapor during ACE-Asia using airborne sun photometer and airborne in situ and ship-based lidar measurements. J. Geophys. Res. 108, 8656 (doi:10.1029/ 2002JD003361).

Shaw, G.E., 1976. Error analysis in multi-wavelength sun photometry. Pure Appl. Geophys. 114, 1–14.

Shettle, E.P., and Anderson, S.M., 1995. New visible and near IR ozone absorption cross-sections for MOD-TRAN. In: Anderson, G.P., Picard, R.H., Chetwynd, J.H. (Eds.), Proceedings of the 17th Annual Review Conference on Atmospheric Transmission Models, 8–9 June 1994. Phillips Laboratory, Bedford. Publication PL-TR-95-2060, Special Reports No. 274, pp. 335–345.

Thome, K.J., Herman, B.M., Reagan, J.A., 1992. Determination of precipitable water from solar transmission. J. Appl. Meteorol. 31, 157–165.

Turner, D.D., Lesht, B.M., Clough, S.A., Liljegren, J.C., Revercomb. H.E., Tobin, D.C., 2003. Dry bias and variability in VAISALA RS80-H radiosondes: the ARM experience. J. Atmos. Ocean. Tech., 20 (1), 117–132.

Vogelmann, A.M., Ramanathan, V., Conant, W.C., Hunter, W.E., 1998. Observational constraints on non-Lorentzian continuum effects in the near-infrared solar spectrum using ARM ARESE data. J. Quant. Spectrosc. Radiat. Transfer 60, 231–246.

Volz, F.E., 1974. Economical multispectral Sun photometer for measurements of aerosol extinction from 0.44 to 1.6 μm and precipitable water. Appl. Opt. 13, 1732–1733.